ACS Catalysis

pubs.acs.org/acscatalysis Research Article

Role of an Inert Electrode Support in Plasmonic Electrocatalysis

Sagar Ganguli and Alina Sekretareva*

Cite This: ACS Catal. 2022, 12, 4110–4118 Read Online

ACCESS | Metrics & More | Article Recommendations | Supporting Information

ABSTRACT: Direct loading of plasmonic nanostructures onto catalytically inert conductive support materials leads to the Schottky barrier-free architecture of the photocatalytic system. Such systems have recently attracted the attention of the research community as they permit collection of hot carriers independent of their energy when additional charge separation strategies are used. However, a systematic mechanistic investigation and description of the contribution of an inert conductive support to plasmonic electrocatalysis is missing. Herein, we systematically investigated the effect of the supporting electrode material on the observed photoinduced enhancement by comparing the photoelectrocatalytic properties of AuNPs supported on highly oriented pyrolytic graphite (HOPG) and indium tin oxide (ITO) electrodes using electrocatalytic benzyl alcohol (BnOH) oxidation as a model system. Upon illumination, only ~(3 ± 1)% enhancement in catalytic current was recorded on the AuNP/ITO electrodes in contrast to ~(42 ± 6)% enhancement on AuNP/HOPG electrodes. Our results showed that the local heating due to light absorption by the electrode material itself independent of localized surface plasmon effects is the primary source of the observed significant photoinduced enhancement on the HOPG electrodes in comparison to the ITO electrodes. Moreover, we demonstrated that an increased interfacial charge transfer at elevated temperatures and not faster reactant diffusion as suggested previously is the main source of the thermal enhancement. This work highlights the importance of the systematic evaluation of contributions of all parts, even if they are catalytically inert, to the light-induced facilitation of catalytic reactions in plasmonic systems.

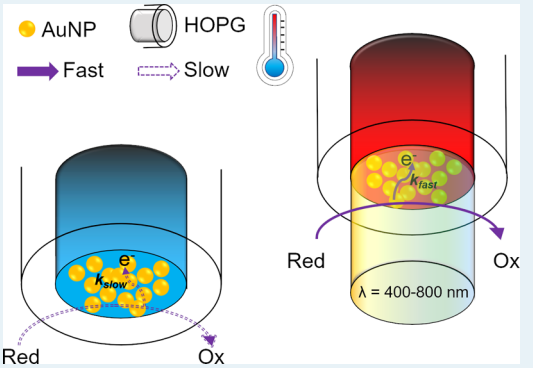

KEYWORDS: *plasmonic electrocatalysis, benzyl alcohol oxidation, graphite electrode support, gold nanoparticles, charge transfer kinetics*

INTRODUCTION

Plasmonic nanostructures (Au, Ag, and Cu) are being increasingly researched as attractive materials for facilitating light-driven heterogeneous catalysis.[1,2] Interaction of the noble metal nanostructures with an incident electromagnetic wave of resonant frequency results in collective oscillation of the confined electrons known as localized surface plasmons (LSPs).[3,4] Nonradiative rapid decay of LSPs through Landau damping leads, first, to the generation of hot charge carriers (electrons and holes) inside the nanostructures within 100 fs. These hot carriers further thermalize inducing a local temperature increase.[5,6] Both these effects, as well as enhanced electric fields near the surface of nanostructures due to LSPs, can contribute to the enhancement of chemical transformation rates in photocatalytic systems based on plasmonic nanostructures.[7−9] Moreover, facilitation of several electrocatalytic reactions, such as alcohol oxidation, water splitting, and carbon dioxide reduction, by LSP effects has been reported.[10,11]

In electrocatalytic systems, plasmonic nanostructures are commonly loaded on support materials to form plasmonic photoelectrodes. The frequently used support materials can be broadly classified into two types: (i) semiconductors, which form a Schottky barrier at the contact with the metallic nanostructures, and (ii) conductive supports that form the continuous energy level. While the Schottky barrier prevents the recombination of charges, its height dictates the limit on energy of charge carriers that can be collected. Photoelectrodes free of the Schottky barrier have recently attracted attention of the research community as they permit to collect hot carriers independent of their energy when additional charge separation strategies are used.[12,13] Among conductive supports, carbon-based materials [glassy carbon (GC), graphene, and graphite] and indium tin oxide (ITO) are the most frequently used in Schottky barrier-free plasmonic systems due to their catalytic inertness. Despite the great interest in designing the Schottky barrier-free systems with maximized hot carrier utilization, the role of the catalytically inert electrode support in photocurrent enhancement is discussed only in a few reports. For example, Shi et al. reported that the photothermal contribution to the photocurrent of oxygen reduction reaction on Ag nanostruc-

Received: January 12, 2022
Revised: March 10, 2022
Published: March 18, 2022

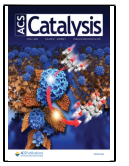

tures could be minimized by using graphene as a support.[14] Liao and co-workers attributed the enhancement of glucose electro-oxidation under irradiation on a reduced graphene oxide (rGO)−AuNP GC composite electrode to the excellent electron transfer capability of rGO facilitating hot charge carrier separation.[15] Kim's group proposed that rGO contributes to the significant enhancement of photocatalytic activity of AuNPs/Pd/rGO toward oxygen evolution and hydrogen evolution reactions by mediating hot-electron transfer to catalytic sites on Pd.[16] All these reports suggest a positive effect of carbon-based materials, particularly with a sp^2 carbon structural motif, on the charge separation process leading to increased photocurrents in electrocatalytic systems. However, the systematic mechanistic investigation and description of the inert electrode support contribution to plasmonic electrocatalysis is missing.

Here, we systematically investigate the effect of the supporting electrode material on the observed photocatalytic enhancement and its role in facilitating charge separation at illuminated electrodes. We compare photoelectrocatalysis by AuNPs supported on highly oriented pyrolytic graphite (HOPG), a sp^2 carbon-based material with a multilayer graphene structure with minimum defects,[17] and on ITO using electrocatalytic benzyl alcohol (BnOH) oxidation as a model system. Employing voltammetry [linear sweep (LSV) and cyclic (CV)], photocurrent measurements at various wavelengths, temperature variation studies, and hydrodynamic voltammetry, we show that the local heating due to light absorption by the electrode material itself independent of LSP effects is the primary source of the observed significant photoinduced enhancement on the carbon-based electrodes in comparison to ITO. Moreover, we demonstrate that faster charge transfer from the electrode to the reactant molecule at elevated temperatures, and not faster reactant diffusion is the main source of the enhancement. This work highlights the importance of systematic evaluation of contributions of all parts, even if they are catalytically inert, to the light-induced facilitation of catalytic reactions in plasmonic systems.

EXPERIMENTAL SECTION

Materials. AuNPs (20 nm diameter; OD 1, stabilized suspension in 0.1 mM PBS, reactant free), $[Ru(NH_3)_6]Cl_2$, and BnOH were purchased from Sigma-Aldrich. Sodium carbonate (Na_2CO_3) and sodium bicarbonate ($NaHCO_3$) were procured from Merck. HOPG rod (diameter: 0.2 cm) was purchased from Goodfellow and embedded in a Teflon sheath keeping only the top surface exposed. Both counter (Pt ring) and reference [Ag/AgCl; 1 (M) KCl] electrodes were purchased from CH Instruments. An ITO-covered glass (8−12 Ω/cm^2) was procured from Redoxme AB. The green (325 mW/cm^2, 532 nm), blue (206 mW/cm^2, 405 nm), and red (266 mW/cm^2, 650 nm) lasers were purchased from Lucinda. The carbon-coated copper TEM grid was procured from Agar Scientific.

Transmission Electron Microscopy Measurements. Transmission electron microscopy (TEM) measurements were carried out using a FEI Tecnai F30 ST 300 kV field emission gun TEM/STEM instrument equipped with a Gatan imaging filter, energy-dispersive detector, high-angle annular dark-field detector, Lorentz lens, and bi-prism for electron holography. The TEM samples were prepared by depositing a drop of the as-received AuNP suspension on a carbon-coated copper TEM grid and dried at room temperature for several hours before examination in TEM.

UV−Vis Absorption Spectroscopy Measurements. First, the as-received AuNP suspension was diluted 100 times with deionized water. The resulting suspension was then transferred to a cuvette with a path length of 1 cm and spectroscopic measurements were carried out in the medium-scan mode of Varian Cary 50 Bio UV−visible spectrophotometer. The wavelength range and slit-width were 800−400 and 3 nm, respectively. For solid-state measurements, 5 μL of as-received AuNP solution was drop-cast on the HOPG substrate and an ITO-covered glass, followed by drying under ambient conditions. The AuNP-coated ITO-covered glass and the bare ITO-covered glass were placed in the light path of the spectrometer using a holder, and measurements were performed with the same parameters. For the HOPG and the AuNP-coated HOPG, we performed diffuse reflectance spectroscopy (DRS) in the medium-scan mode of the Varian Cary 4000 UV−visible spectrophotometer using Internal DRA 900 accessory. The obtained % reflectance (% R) data were converted into absorbance (A_{10}) using the following equation[18]

$$A_{10} = -\log_{10}\left(\frac{\%R}{100}\right) \quad (1)$$

Electrode Preparation. 5 μL of AuNPs suspension was carefully drop-cast on a polished HOPG (diameter: 0.2 cm; embedded in Teflon) electrode. It was then left overnight for drying to obtain the AuNP-coated HOPG (AuNP/HOPG) electrode. A similar protocol was followed to develop a AuNP-coated ITO electrode (AuNP/ITO), where 40 μL of AuNP suspension was drop-cast on 0.5 cm^2 of an ITO-covered glass. Thereafter, a nonconductive resin was applied on AuNP/ITO electrodes, leaving exposed an area corresponding to the laser diameter (0.2 cm). This ensured that the obtained electrochemical data are not convoluted by any background current and that illuminated areas for both HOPG and ITO electrodes are the same.

Electrochemical Measurements. A three-electrode cell setup using AuNP/HOPG or AuNP/ITO as a working, Pt as a counter, and Ag/AgCl [1 (M) KCl] as a reference electrode was employed to perform electrochemical measurements. 50 mL of 0.1 (M) carbonate-bicarbonate buffer (pH ∼ 10.6) was used as the electrolyte. The electrochemical experiments were performed using Gamry Reference 600 and Ivium CompactStat.h electrochemical workstations. Prior to performing electrocatalytic BnOH oxidation measurements, the AuNP/HOPG electrode was subjected to 15 cycles of CV at 50 mV/s between 0.45 and 1.5 V versus RHE to obtain a kinetically stable state. Thereafter, 100 μL of BnOH was added to the electrolyte and stirred till its complete dissolution to make 20 mM BnOH solution. In this solution, the electrode was again subjected to 15 cycles of CV in the same potential range at 50 mV/s before conducting measurements for data interpretation. LSV/CV were performed in the same potential window at 50 mV/s inside a Faraday cage under dark and light to evaluate the electrocatalytic performance. For excitation power-dependent studies the lasers of different wavelengths were used. The maximum intensities of the lasers were 206 mW/cm^2, 325 mW/cm^2, and 266 mW/cm^2 for 405 nm, 532 nm, and 650 nm, respectively. The excitation power of the lasers was tuned using a Thorlabs step variable neutral density optical filter.

https://doi.org/10.1021/acscatal.2c00206
ACS Catal. 2022, 12, 4110−4118

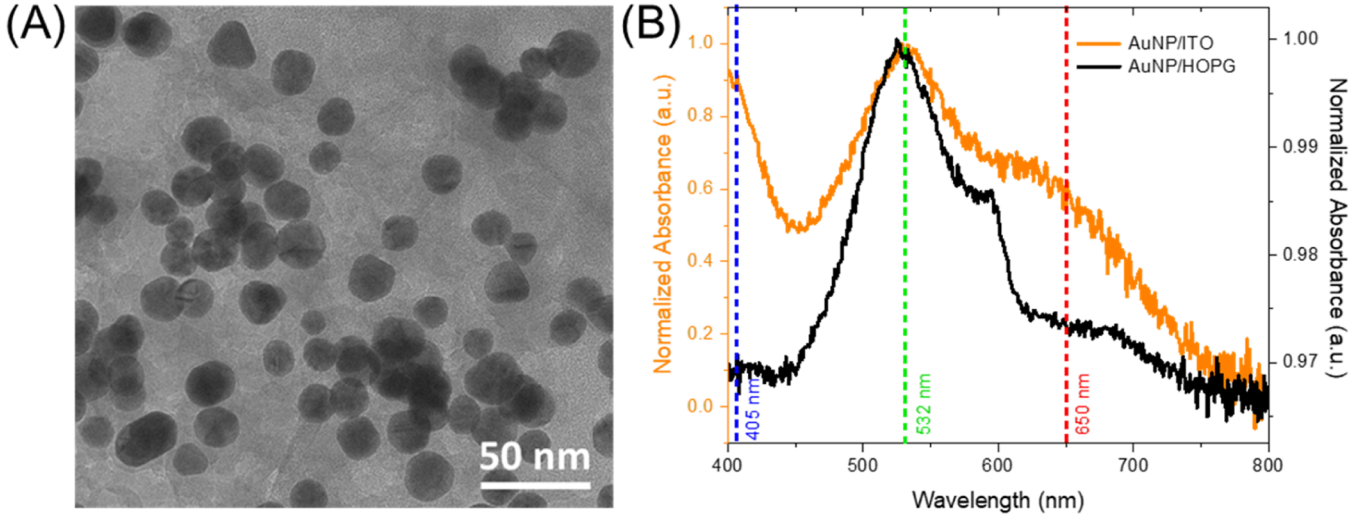

Figure 1. (A) TEM image of as-received reactant-free AuNPs with an average particle size of (18 ± 4) nm. (B) UV−vis absorption spectroscopy measurements of dried AuNPs drop-cast on an ITO-covered glass (orange trace) and HOPG substrate (black trace). The dashed lines indicate the wavelengths of the lasers used in plasmonic electrocatalysis measurements (vide infra).

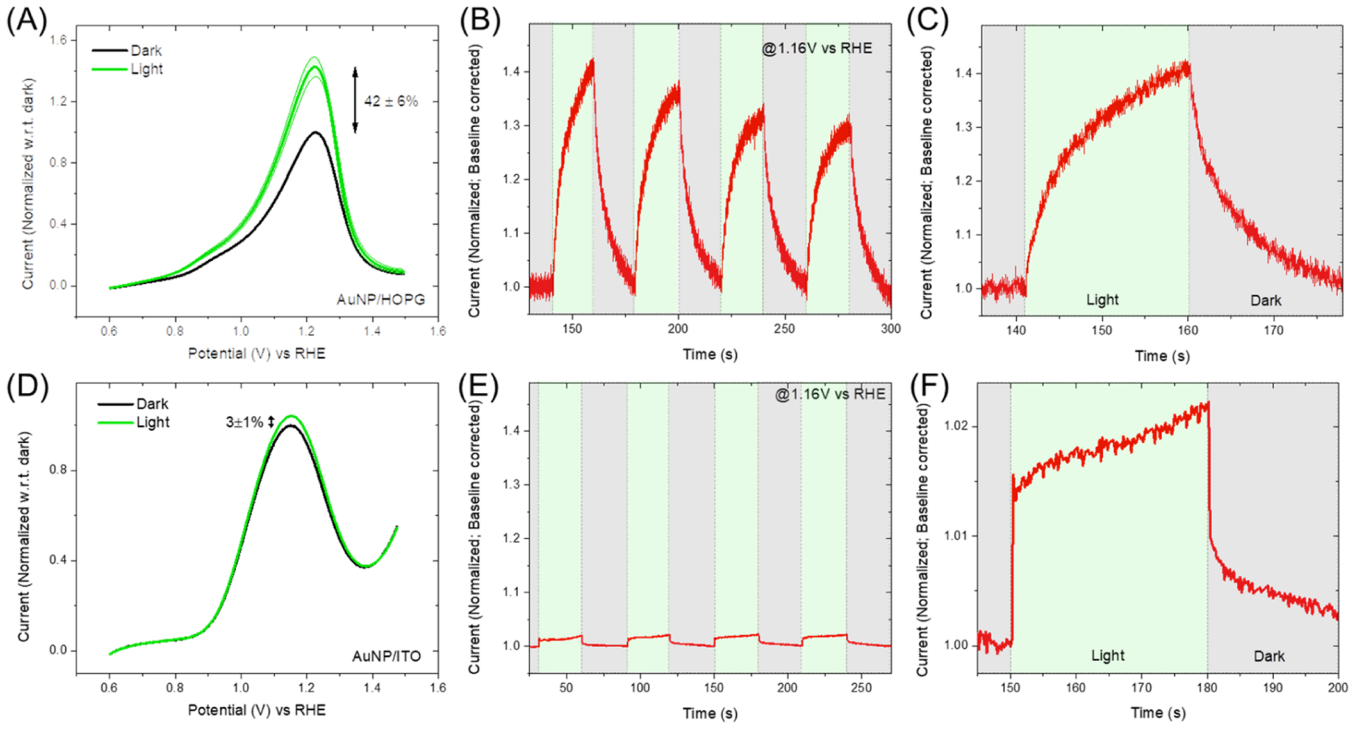

Figure 2. LSV scans on (A) AuNP/HOPG and (D) AuNP/ITO electrodes in 20 mM BnOH solution in the dark (black trace) and under illumination (green trace). The voltammograms were recorded thrice to compute the mean values and the standard deviations. The standard deviations for currents recorded under illumination at different applied potentials are shown as a shaded region. The population mean value and the corresponding standard deviation are indicated. Chronoamperometry measurements on (B,C) AuNP/HOPG and (E,F) AuNP/ITO electrodes in 20 mM BnOH solution under alternating illumination at a fixed applied potential of 1.16 V vs RHE. Illumination source: 532 nm laser (325 mW/cm^2).

RESULTS AND DISCUSSION

Characterization of AuNPs. Reactant-free AuNPs with an average size of (18 ± 4) nm as characterized by TEM measurements (Figure 1A) have been used throughout this study. The AuNP suspension showed a single, sharp absorption band with an absorption maximum at 518 nm (Figure S1). This is consistent with the dipole LSP resonance band of free electrons in spherical AuNPs.[19] The additional absorption features at lower (<470 nm) wavelengths can be attributed to interband transitions in AuNPs.[20] For AuNPs supported on HOPG and ITO electrodes, the highest intensity peaks were observed at 532 nm, characteristic of the dipole LSPR band of free electrons in a spherical AuNP (Figure 1B). This suggests that the majority of the AuNPs are in a nonagglomerated state. Additional broad bands of lower intensity observed at higher wavelengths for both electrodes can be attributed to the near-field interaction between neighboring AuNPs.[21,22] This generally arises when AuNPs

https://doi.org/10.1021/acscatal.2c00206
ACS Catal. 2022, 12, 4110−4118

are in close proximity due to the formation of small clusters under solid-state conditions. Thus, while there is a minor agglomeration and cluster formation for immobilized AuNPs, the majority of AuNPs drop-cast on the electrodes remain in a nonagglomerated state.

Photoelectrocatalytic Benzyl Alcohol Oxidation on AuNPs. The electrocatalytic activity of AuNPs supported on HOPG and ITO electrodes toward BnOH oxidation in the dark and under continuous-wave illumination using a selected laser excitation source light was investigated. The AuNP-modified electrodes served as the working electrode in a three-electrode setup. The surface area of the AuNP catalytic layer exposed to solution was the same for both AuNP/HOPG and AuNP/ITO electrodes. The entire exposed catalyst layer was illuminated by a light source placed at the bottom or at the front of the transparent cell for the AuNP/HOPG (Figure S2) and AuNP/ITO electrodes (Figure S3), respectively. Figure 2A,D show LSVs recorded on the AuNP/HOPG and AuNP/ITO electrodes, respectively, in 20 mM BnOH solution in the dark (black curves) and under irradiation with a 532 nm laser with the intensity of 325 mW/cm^2 (green curves). A distinct oxidation peak was observed on both electrodes in the dark (at 1.24 V vs RHE for AuNP/HOPG and at 1.15 V vs RHE for AuNP/ITO). Bare HOPG and ITO electrodes did not demonstrate significant catalytic activity toward BnOH oxidation compared to the AuNP-modified electrodes (Figures S4 and S5, respectively). Thus, the observed anodic peaks were ascribed to BnOH oxidation on the AuNPs serving as catalytic centers.[23]

Upon illumination, a striking difference in the photocurrent responses was observed for the AuNPs supported on the HOPG and the ITO electrodes. Only ∼(3 ± 1)% peak current enhancement upon irradiation with the 532 nm laser (325 mW/cm^2) was recorded on the AuNP/ITO electrodes in 20 mM BnOH solution in contrast to ∼(42 ± 6)% enhancement on the AuNP/HOPG electrodes (Figure 2A,D). To understand the primary reason for the observed difference in the photocurrent responses and the source of the significant enhancement on the HOPG electrodes, we performed chronoamperometry measurements under alternating illumination [532 nm laser (325 mW/cm^2)] at a fixed applied potential of 1.16 V versus RHE. Prior to switching on illumination, the electrodes were kept at the fixed potential to establish a stable dark current. Figure 2B,C shows the photocurrent response of the AuNP/HOPG electrode in 20 mM BnOH solution. Upon switching on illumination (green areas in Figure 2B,C), an increase of the anodic current is observed. Subsequent switching of the light source (gray areas in Figure 2B,C) results in a decrease of the current back to the dark value. Both an increase of the photocurrent upon irradiation and a subsequent decrease when the light was off were gradual lasting over 20 s before reaching a steady-state value.

The photocatalytic enhancement of alcohol oxidation on plasmonic nanostructures supported on carbon-based materials has been previously attributed to the participation of hot charge carriers generated during plasmon decay.[24−26] The lifetime of hot carriers generated due to Landau damping of the plasmons in AuNPs does not exceed 1 ps.[5,27,28] Thus, for the photocurrent resulting from the participation of hot carriers in the catalytic reaction, one would expect a sharp decrease of the signal upon switching off illumination. Indeed, it has been demonstrated previously that a fast-decaying component of the photocurrent upon switching off illumination can be attributed to hot carriers, while a slow-decaying component to thermal effects.[29−31] We would like to note here that the time constant (τ) of the cell should be measured to perform such an analysis. The time constant of the cell, defined as a product of the cell resistance (R_s) and the double-layer capacitance (C_{dl}), represents the minimum time the cell requires to establish a reliable current signal after perturbations in the double-layer. Any conclusions on values of the photocurrent can be drawn only from current measured at time scales larger than τ. This value can be readily measured.[32] To measure τ, first, a potential in the non-Faradaic region (0.65 V vs RHE) was held for 20 s to reach a steady-state current, followed by applying a small potential step (10, 20, and 30 mV, respectively) (Figure S6). This potential step (E) led to a sharp increase in the current corresponding to the charging of the double layer. This charging current thereafter decays according to eq 2

$$i = \frac{E}{R_s} \cdot e^{-t/R_s C_{dl}} \tag{2}$$

where i and t are current and time, respectively. The time required for the current to reach ∼37% of its initial value represents the τ of the electrochemical system.[32] The obtained value of the τ for the AuNP/HOPG electrodes is ∼30 ms (Figure S6A−C). The slow decay of the BnOH oxidation photocurrent on the AuNP/HOPG electrodes (Figure 2B,C) over a time greater than the five cell time constants (5τ) undermines the direct participation of hot carriers in the catalytic reaction. This is in agreement with the recently reported finding by Nocera et al. that ps-range lifetimes of excited states are orders of magnitude shorter than that required for productive photochemistry.[33] Thus, the observed slow decay of the photocurrent suggests that heating is the primary source of the photocurrent on the AuNP/HOPG electrodes.

Figure 2E,F displays the photocurrent response of the AuNP/ITO electrode under alternating illumination [532 nm laser (325 mW/cm^2)] in 20 mM BnOH solution. Similar to AuNP/HOPG electrodes, the increase and the decay of the anodic photocurrent coincide with switching on (green areas in Figure 2E,F) and off (gray areas in Figure 2E,F) the light source. Interestingly, the nature of the current change is starkly different from the AuNP/HOPG electrodes as light on/off led to ∼1.5% instantaneous (∼200 ms) rise/drop in the current, followed by a slower change (Figure 2E,F) for up to ∼2.2% of the total current increase. As the τ for the AuNP/ITO system was determined to be 870 ms (Figure S6D), the observed instantaneous photocurrent response can not be fully attributed to the direct participation of hot carriers in the reaction because part of the charge goes to charging of the double layer changed due to illumination. This suggests that any contribution of hot carriers for the AuNP/ITO system is lower than 1.5%. The remaining 0.7% current increase occurring over seconds (at timescales much higher than the cell constant) can be ascribed to local heating due to thermalization of hot carriers within AuNPs.

Temperature Effects on AuNP/HOPG versus AuNP/ITO Electrodes. The significantly higher value of the photocurrent on the AuNP/HOPG in comparison to the AuNP/ITO electrodes attributed to temperature effects (42% on the HOPG electrodes compared to 0.7% on the ITO electrodes as discussed above) invokes the question of whether

https://doi.org/10.1021/acscatal.2c00206
ACS Catal. 2022, 12, 4110−4118

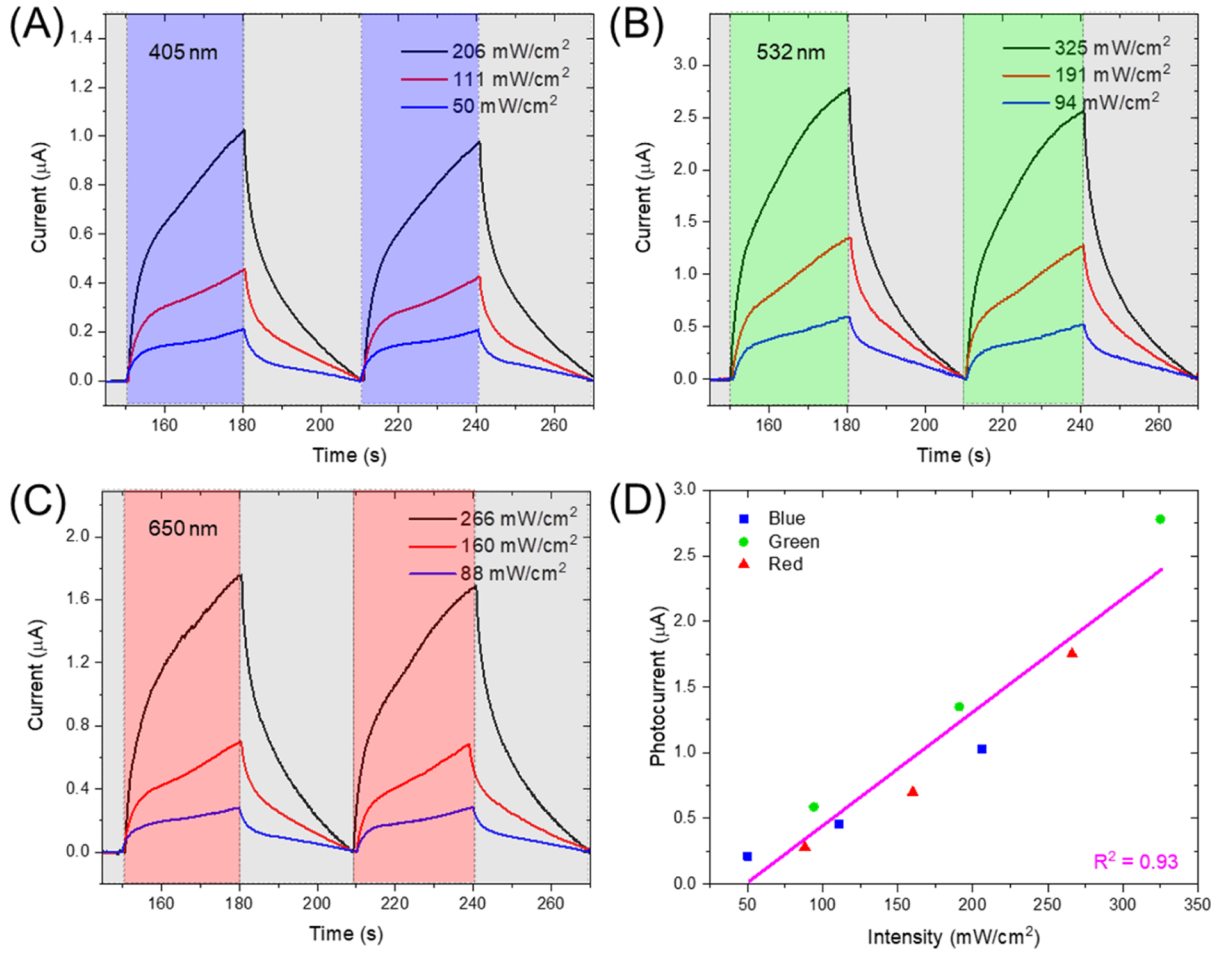

Figure 3. Chronoamperometry measurements on the AuNP/HOPG electrodes in 20 mM BnOH solution at a fixed applied potential of 1.16 V vs RHE under alternating illumination of different intensities with (A) 405, (B) 532, and (C) 650 nm lasers. (D) Dependence of the photocurrent response on intensity at different wavelengths.

the local heating due to the decay of hot carriers within AuNPs or HOPG itself, plays the key role in the photo-assisted enhancement. Because the temperature rise is proportional to the total amount of absorbed optical energy,[34] the photocurrent response should reproduce the absorption spectrum of the material responsible for the heating. We performed excitation power and wavelength-dependent chronoamperometry measurements under alternating illumination (30 s light on/off) on the AuNP/HOPG electrodes in 20 mM BnOH solution. Figure 3A–C shows the dependence of the photocurrent on the excitation power for illumination with blue (405 nm, A), green (532 nm, B), and red (650 nm, C) lasers. The AuNP/HOPG electrodes displayed identical in shape photoresponses under illumination with the light sources of different wavelengths. To determine the values of the photocurrent at different wavelengths and intensities, the current recorded at the end of each dark period was used to create a baseline. After subtracting the baseline from the entire chronoamperometry data, the current recorded at 30 s of irradiation was considered as the photocurrent at a particular wavelength and intensity. The dependence of the photocurrent on the illumination intensity for different wavelengths is shown in Figure 3D. Photocurrent values at different intensities for different wavelengths can be fitted to a single line with an acceptable goodness-of-fit value (R^2 = 0.93), suggesting that there is no strong dependence of the photocurrent on the wavelength of the incident light. If the plasmonic effects on AuNPs were the primary source of the photocurrent, one would expect the photoresponse to be highly wavelength-dependent with the enhancements coinciding with the LSP resonance features of the surface-adsorbed AuNPs (Figure 1B, black trace). We performed DRS measurements of the HOPG substrate to understand its absorption behavior. The % reflectances at 405, 532, and 650 nm were found to be 12.96, 11.80, and 11.05, respectively (Figure S7). Such close % reflectance values confirm that HOPG absorbs across the visible spectrum with a near-equal extinction coefficient.[35,36] Thus, the wavelength independence of the photocurrent suggests that the heating of the HOPG electrode itself due to absorption of the incident light is the primary source of the BnOH oxidation photo-enhancement on the AuNP/HOPG electrodes.

To further confirm that the light absorption by the HOPG electrode results in the temperature increase, we compared the CV of the bare HOPG electrodes in buffer recorded under light illumination with the 532 nm (325 mW/cm^2) laser (Figure S8A) to the CV curves recorded in the dark at different temperatures of buffer solution varied externally using a thermostat (Figure S8B). As can be seen from a comparison of Figure S8A,B, increasing temperature leads to the similar changes in CV curves as the illumination. Specifically, an increase of cathodic current at ~0.4 V versus RHE due to

https://doi.org/10.1021/acscatal.2c00206
ACS Catal. 2022, 12, 4110–4118

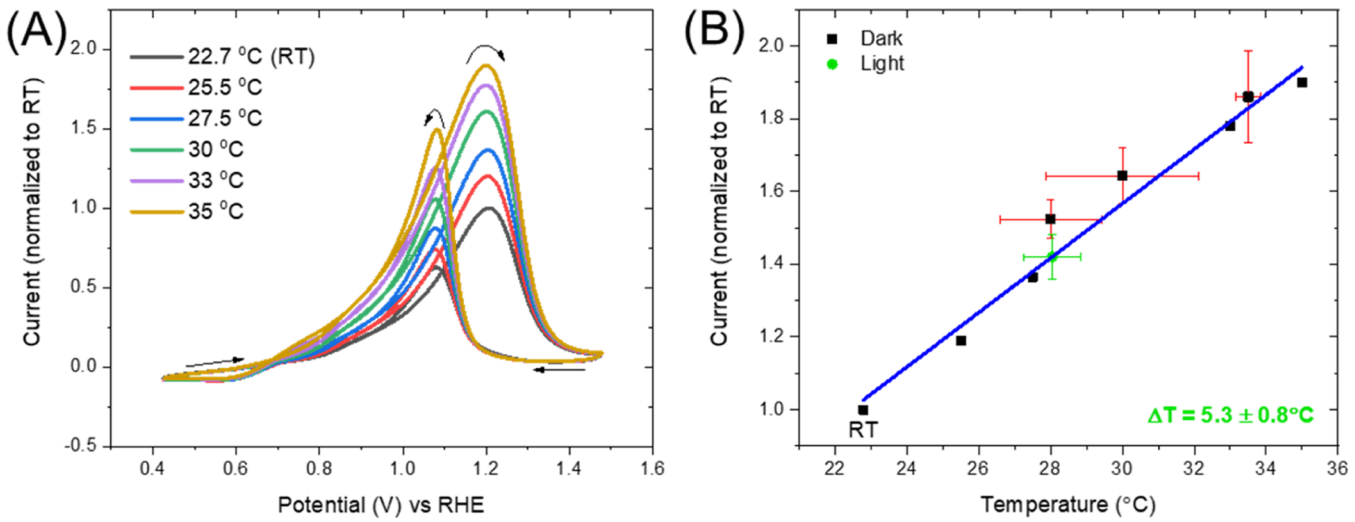

Figure 4. (A) CV scans (normalized to room temperature) on AuNP/HOPG electrodes in 20 mM BnOH solution at different temperatures in the dark. (B) Determination of the temperature increase under irradiation (532 nm, 325 mW/cm^2; green point) from a calibration curve drawn using forward scan peak currents recorded at various temperatures. The voltammograms were recorded thrice to compute the population mean value and the corresponding standard deviation.

oxygen reduction reaction on the HOPG electrode and a decrease of the anodic current at ∼1.4 V versus RHE are observed upon illumination and with the increase in the temperature of buffer solution. A similar observation for an illuminated AuNP/HOPG electrode and its temperature-dependent response also confirm that the light absorption by HOPG is the primary source of the temperature increase (Supporting Note 1; Figure S9).

In contrast to HOPG, ITO-covered glass has a high transmittance across the visible range (Figure S10).[37] Therefore, the tepid (2.2%) photoresponse on the AuNP/ITO electrodes originated only from light absorption by AuNPs.

To quantify the effective change in temperature due to irradiation, we performed BnOH electrooxidation on the AuNP/HOPG electrodes in the dark at various temperatures of solution controlled externally by a thermostat (Figure 4A). The measurements were repeated thrice at each temperature and statistical analysis was performed to obtain the average current and error values. The anodic peak current on the forward scan was found to increase linearly with the temperature (Figure 4B). Using the peak current dependence on the temperature as a calibration curve, the effective temperature increase upon irradiation with the 532 nm (325 mW/cm^2) laser was found to be 5.3 ± 0.8 °C. This further explains the apparent linear dependence of the photocurrent on laser intensity instead of the exponential dependence expected for temperature effects. The narrow range of temperature changes is not sufficient to distinguish between linear and exponential functions.[38] We further considered how the temperature increase affects the kinetics of BnOH electrooxidation.

Mechanistic Investigation of Temperature Effects on Benzyl Alcohol Electrooxidation. In the plasmonic electrocatalysis literature, enhanced photocurrent at increased temperatures has generally been associated with higher diffusion of reactants and products at the catalyst/electrolyte interface due to significant local heating.[24,39] The diffusion-controlled peak current (i_p) for an irreversible electrochemical process, such as BnOH electrooxidation, can be described by the Delahay equation (eq 3)[40,41]

$$i_p = 0.282nC_bA\sqrt{\frac{\pi F\alpha nD\nu}{RT}} \quad (3)$$

where n is the number of electrons, F is Faraday's constant (96,485 C/mol), C_b is the bulk concentration of the reactant, A is the surface area of the electrode, D is the diffusion coefficient of the reactant, R is the universal gas constant, α is the transfer coefficient, ν is the scan rate, and T is the temperature. The equation predicts the linear dependence of the i_p on the square root of the ν and zero intercept for the i_p (corrected for capacitive current contribution) versus $\nu^{1/2}$ line. Figure S11A,C shows CVs of BnOH oxidation on the AuNP/HOPG electrodes at different ν values in the dark and under illumination with the 532 nm (325 mW/cm^2) laser, respectively. Though the i_p versus $\nu^{1/2}$ relationship was linear (Figure S11B,D), the intercepts in both cases were nonzero, suggesting a mixed control of the peak current.

To probe the effect of mass transfer on the current, we performed hydrodynamic voltammetry measurements on rotating disk AuNP/HOPG electrodes (RDEs) in 20 mM BnOH solution in the dark at varied rotation speeds (0−2500 rpm). As expected for a mass-transport controlled reaction, the current increases with the increase in the rotation speed. However, it does not reach a steady-state value even at high overpotentials (Figure 5A). In contrast to stationary electrodes, the mass transport of BnOH to the rotating electrode surface is both time- and potential-independent and proportional to the $\sqrt{(\text{electrode rotation speed})}$.[42] Therefore, for the mass-transfer-limited process, one would reach a plateau current in RDE measurements once the mass transport of the analyte limits the electrochemical reaction. The peak formation on the AuNP/HOPG electrode in RDE experiments confirms that the electrode process at potentials corresponding to the peak current on the stationary CV is not entirely controlled by diffusion.

By comparing CVs of the AuNP/HOPG electrodes in buffer without and with 20 mM BnOH (Figure S12), we found that the anodic peak corresponding to BnOH oxidation on the forward scan (f) coincides with the commencement of Au oxidation into AuO_x.[23,43] Interestingly, as AuO_x is reduced

https://doi.org/10.1021/acscatal.2c00206
ACS Catal. 2022, 12, 4110−4118

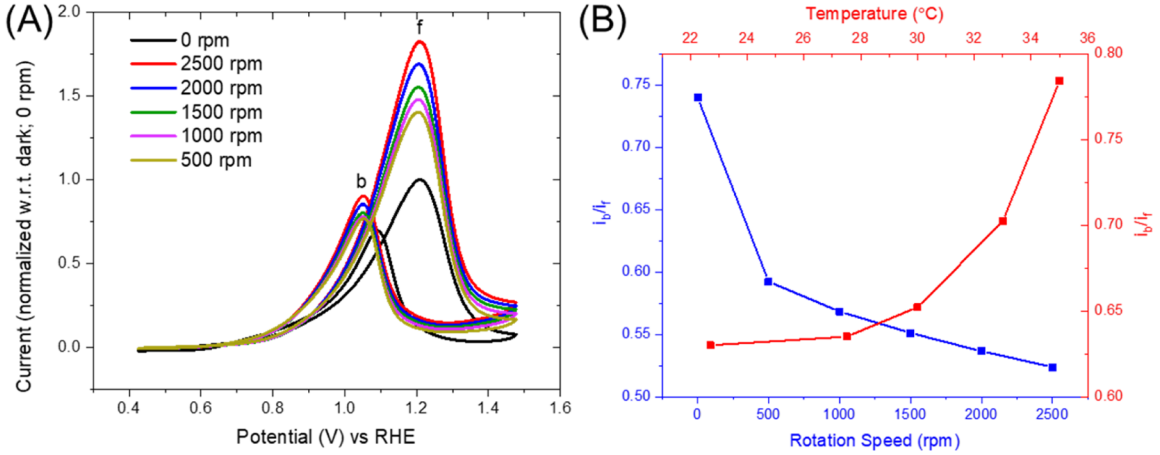

Figure 5. (A) CV scans on AuNP/HOPG electrodes in 20 mM BnOH solution at different rotation speeds in the dark. (B) Dependence of the backward scan peak current (i_b)/forward scan peak current (i_f) ratio determined from the CV curves on the temperature (red trace) and rotation speeds (blue trace).

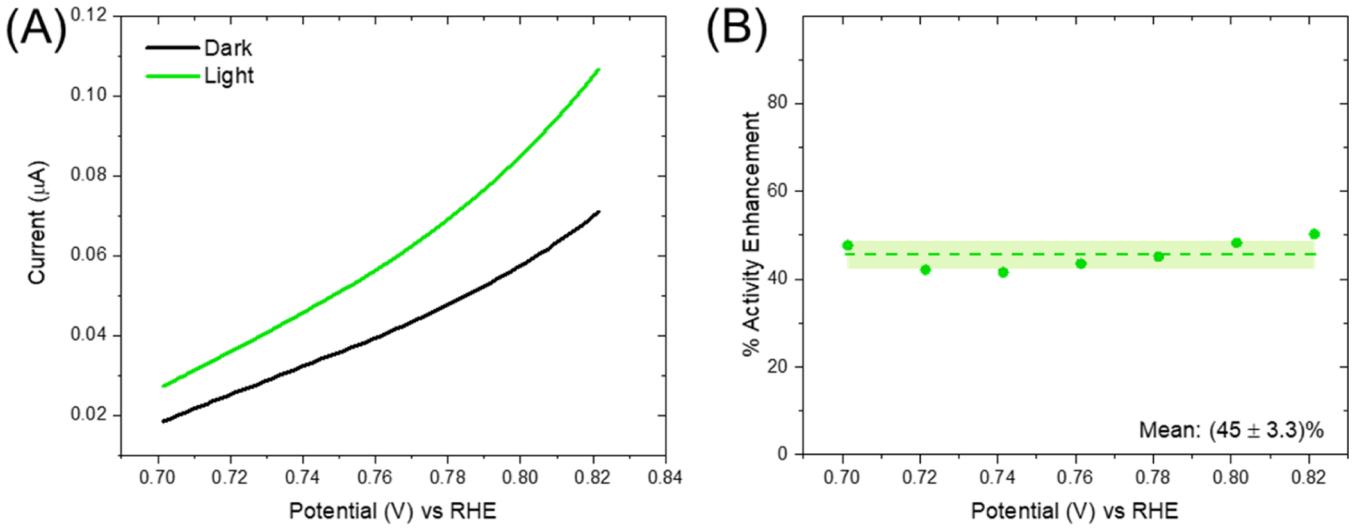

Figure 6. (A) LSV curves on AuNP/HOPG electrodes in 20 mM BnOH solution in the potential region controlled only by charge transfer kinetics (as determined from RDE experiments) in the dark and under illumination (532 nm laser, 325 mW/cm^2), and (B) the photoinduced electrocatalytic activity enhancement determined from (A) as a ratio of current under illumination to the dark current. The voltammograms were recorded thrice to compute the mean values and corresponding standard deviations. The standard deviations at different potentials are shown as a shaded region. The population mean value and the corresponding standard deviation are indicated.

back to Au on the backward scan (*b*), the reemergence of the BnOH electrooxidation current is observed. This suggests that the oxidation of AuO_x leads to the loss of the catalytically active Au surface, resulting in the peak formation on the forward scan.

The mixed-controlled nature of the peak current, as was observed for BnOH electrooxidation on the AuNP/HOPG surface, implies that the electrocatalytic activity can increase if either diffusion or charge transfer rates or both increase. To probe the effect of irradiation on diffusion rates, we performed CV measurements on the AuNP/HOPG electrodes in 1 mM solution of $Ru(NH_3)_6Cl_2$ in 1 M KCl in the dark and under illumination with the 532 nm (325 mW/cm^2) laser (Figure S13A). $Ru(NH_3)_6Cl_2$ is a reversible redox probe with fast electrode kinetics and the CV peak currents entirely controlled by mass transport (diffusion).[32,44] Therefore, the change in the peak current can provide a quantitative estimate of diffusion enhancement due to heating upon irradiation. As can be seen from Figure S13A, the peak currents of $Ru(NH_3)_6Cl_2$ increased by only 1.6% under irradiation. A similar response was observed in CVs recorded in the dark at increasing temperatures of solution (Figure S13B,C). These results demonstrate that the increased rate of diffusion due to heating cannot explain the ∼42% photocurrent enhancement observed for BnOH oxidation on the AuNP/HOPG electrodes.

As the enhanced diffusion due to local heating was found not to considerably increase the peak current, facilitated charge transfer at higher temperatures should be responsible for improved electrocatalysis. This conclusion is supported by the opposite behavior of the ratio between the backward peak current (i_b) and the forward peak current (i_f) for BnOH oxidation under the temperature variations versus the rotation speed variation in the RDE measurements (Figure 5B). The i_b/i_f ratio decreased with the increase in the rotation speed, as the rotation speed affects only mass transport and the effect of mass transport limitation is higher on i_f compared to i_b. In contrast, i_b/i_f increased with the increase in temperature. This is because i_b is more influenced by charge transfer kinetics than

https://doi.org/10.1021/acscatal.2c00206
ACS Catal. 2022, 12, 4110−4118

i_f and therefore, while the increased temperature led to an increase in both peaks, its effect on i_b was higher compared to i_f.

While the RDE measurements are affected by the Au surface oxidation, they can still be used to identify the current range, where the catalytic activity is entirely charge transfer controlled.[42] In an RDE measurement, any current enhancement with the increase in the rotation speed arises only from the increased mass transport. Thus, the current range that remains unchanged with the increase in the rotation speed is representative of a region entirely controlled by charge transfer kinetics. For the system under study, this current range was found to be 0.018−0.1 μA. We identified the potential window corresponding to this current range under irradiation from Figure 2A. Its comparison with the current recorded in the dark in the same potential window reveals a (45 ± 3.3)% increase of the charge transfer rate under illumination (Figure 6A,B). This enhancement of current is the same within an error to the (42 ± 6)% current enhancement on the forward peak in CV under illumination. We would like to mention that as a rule of thumb, the Arrhenius relationship predicts the doubling of a reaction rate with each 10 °C increase in temperature. Therefore, our observation of (45 ± 3.3)% increase of the charge transfer rate with a temperature increase of ∼5.3 °C arising from illumination is consistent with this prediction. Thus, the increased temperature resulting from light absorption by HOPG facilitates charge transfer kinetics from the electrode to the reactant molecule at the electrode−solution interface.

CONCLUSIONS

We have carried out a systematic investigation of the role of the inert electrode support in photoelectrocatalysis on plasmonic AuNPs. We have noticed a striking difference in the photocurrent responses for AuNPs supported on HOPG and ITO electrodes. The photocurrent on the AuNP/ITO electrodes was 14 times lower than on the AuNP/HOPG electrodes and consisted of two components: a fast-decaying upon switching of illumination component and a slow-decaying component, while the photoresponse of the AuNP/HOPG electrodes had only a slow-decaying component. We found that hot carriers have a negligible contribution to the increased BnOH electrooxidation on AuNPs loaded on the HOPG surface under illumination, and the observed photocurrent resulted from the increased temperature. Moreover, we demonstrated that light absorption by the HOPG substrate and not the recombination of hot carriers in AuNPs is responsible for the temperature increase. Finally, in contrast to previous reports where the effect of increased temperature has only been attributed to higher diffusion of the reactant in the vicinity of the electrode, we showed that the enhancement of catalysis can arise from the increased charge transfer kinetics at elevated temperatures.

This work demonstrated that despite being catalytically inert, carbon-based support materials under illumination can significantly stimulate the electrocatalytic activity of catalytic centers placed on its surface by virtue of their wide spectral absorption. We would like to emphasize that being catalytically inert may not be enough to be chosen as an electrode support for evaluating the true photocatalytic activity of an immobilized catalyst under illumination.

ASSOCIATED CONTENT

Supporting Information

The Supporting Information is available free of charge at https://pubs.acs.org/doi/10.1021/acscatal.2c00206.

Absorption spectroscopy of AuNP suspension, drop-cast AuNPs, and substrates; schematic of electrochemical cells; LSV and chronoamperometry measurements under dark and illumination; scan-rate-dependent CV using AuNP/HOPG; temperature- and illumination-dependent CV of $Ru(NH_3)_6Cl_2$ (PDF)

AUTHOR INFORMATION

Corresponding Author

Alina Sekretareva − *Department of Chemistry, Ångström Laboratory, Molecular Biomimetics, Uppsala University, 75120 Uppsala, Sweden;* orcid.org/0000-0001-7312-0116; Email: alina.sekretareva@kemi.uu.se

Author

Sagar Ganguli − *Department of Chemistry, Ångström Laboratory, Molecular Biomimetics, Uppsala University, 75120 Uppsala, Sweden;* orcid.org/0000-0002-1209-1689

Complete contact information is available at: https://pubs.acs.org/10.1021/acscatal.2c00206

Notes

The authors declare no competing financial interest.

ACKNOWLEDGMENTS

A.S. thanks FORMAS (N 2019-01126) for supporting this research. A.S. and S.G. acknowledge support from Carl Tryggers Stiftelse (N CTS 19:326). A.S. and S.G. thank Petko Chernev for his help with the design of the cell for electrochemical measurements.

REFERENCES

(1) Lang, X.; Chen, X.; Zhao, J. Heterogeneous Visible Light Photocatalysis for Selective Organic Transformations. *Chem. Soc. Rev.* **2013**, *43*, 473−486.

(2) Aslam, U.; Rao, V. G.; Chavez, S.; Linic, S. Catalytic Conversion of Solar to Chemical Energy on Plasmonic Metal Nanostructures. *Nat. Catal.* **2018**, *1*, 656−665.

(3) Kamarudheen, R.; Aalbers, G. J. W.; Hamans, R. F.; Kamp, L. P. J.; Baldi, A. Distinguishing Among All Possible Activation Mechanisms of a Plasmon-Driven Chemical Reaction. *ACS Energy Lett.* **2020**, *5*, 2605−2613.

(4) Ezendam, S.; Herran, M.; Nan, L.; Gruber, C.; Kang, Y.; Gröbmeyer, F.; Lin, R.; Gargiulo, J.; Sousa-Castillo, A.; Cortés, E. Hybrid Plasmonic Nanomaterials for Hydrogen Generation and Carbon Dioxide Reduction. *ACS Energy Lett.* **2022**, *7*, 778−815.

(5) Yu, S.; Wilson, A. J.; Kumari, G.; Zhang, X.; Jain, P. K. Opportunities and Challenges of Solar-Energy-Driven Carbon Dioxide to Fuel Conversion with Plasmonic Catalysts. *ACS Energy Lett.* **2017**, *2*, 2058−2070.

(6) Zhan, C.; Moskovits, M.; Tian, Z.-Q. Recent Progress and Prospects in Plasmon-Mediated Chemical Reaction. *Matter* **2020**, *3*, 42−56.

(7) Zhang, Y.; He, S.; Guo, W.; Hu, Y.; Huang, J.; Mulcahy, J. R.; Wei, W. D. Surface-Plasmon-Driven Hot Electron Photochemistry. *Chem. Rev.* **2018**, *118*, 2927−2954.

(8) Cortés, E.; Besteiro, L. V.; Alabastri, A.; Baldi, A.; Tagliabue, G.; Demetriadou, A.; Narang, P. Challenges in Plasmonic Catalysis. *ACS Nano* **2020**, *14*, 16202−16219.

(9) Linic, S.; Chavez, S.; Elias, R. Flow and Extraction of Energy and Charge Carriers in Hybrid Plasmonic Nanostructures. *Nat. Mater.* **2021**, *20*, 916−924.
(10) Zhao, J.; Xue, S.; Ji, R.; Li, B.; Li, J. Localized Surface Plasmon Resonance for Enhanced Electrocatalysis. *Chem. Soc. Rev.* **2021**, *50*, 12070−12097.
(11) Chen, D.; Zhang, R.; Wang, R.; Negro, L. D.; Minteer, S. D. Gold Nanofiber-Based Electrodes for Plasmon-Enhanced Electrocatalysis. *J. Electrochem. Soc.* **2016**, *163*, H1132.
(12) Robatjazi, H.; Bahauddin, S. M.; Doiron, C.; Thomann, I. Direct Plasmon-Driven Photoelectrocatalysis. *Nano Lett.* **2015**, *15*, 6155−6161.
(13) Tian, Y.; Tatsuma, T. Mechanisms and Applications of Plasmon-Induced Charge Separation at TiO2 Films Loaded with Gold Nanoparticles. *J. Am. Chem. Soc.* **2005**, *127*, 7632−7637.
(14) Shi, F.; He, J.; Zhang, B.; Peng, J.; Ma, Y.; Chen, W.; Li, F.; Qin, Y.; Liu, Y.; Shang, W.; Tao, P.; Song, C.; Deng, T.; Qian, X.; Ye, J.; Wu, J. Plasmonic-Enhanced Oxygen Reduction Reaction of Silver/Graphene Electrocatalysts. *Nano Lett.* **2019**, *19*, 1371−1378.
(15) Liao, X. W.; Wang, S. S.; Xu, G. Y.; Wang, C. Enhanced Electrocatalysis via Boosted Separation of Hot Charge Carriers of Plasmonic Gold Nanoparticles Deposited on Reduced Graphene Oxide. *ChemElectroChem* **2019**, *6*, 1419−1426.
(16) Lee, J.-E.; Marques Mota, F.; Choi, C. H.; Lu, Y.-R.; Boppella, R.; Dong, C.-L.; Liu, R.-S.; Kim, D. H. Plasmon-Enhanced Electrocatalytic Properties of Rationally Designed Hybrid Nanostructures at a Catalytic Interface. *Adv. Mater. Interfaces* **2019**, *6*, 1801144.
(17) Pumera, M. Graphene-Based Nanomaterials and Their Electrochemistry. *Chem. Soc. Rev.* **2010**, *39*, 4146−4157.
(18) Dahm, K. D.; Dahm, D. J. Principles of Diffuse Reflectance Spectroscopy. *Handbook of Near-Infrared Analysis*; Routledge Handbooks Online, 2021.
(19) Eustis, S.; El-Sayed, M. A. Why Gold Nanoparticles Are More Precious than Pretty Gold: Noble Metal Surface Plasmon Resonance and Its Enhancement of the Radiative and Nonradiative Properties of Nanocrystals of Different Shapes. *Chem. Soc. Rev.* **2006**, *35*, 209−217.
(20) Balamurugan, B.; Maruyama, T. Evidence of an Enhanced Interband Absorption in Au Nanoparticles: Size-Dependent Electronic Structure and Optical Properties. *Appl. Phys. Lett.* **2005**, *87*, 143105.
(21) Scheeler, S. P.; Mühlig, S.; Rockstuhl, C.; Hasan, S. B.; Ullrich, S.; Neubrech, F.; Kudera, S.; Pacholski, C. Plasmon Coupling in Self-Assembled Gold Nanoparticle-Based Honeycomb Islands. *J. Phys. Chem. C* **2013**, *117*, 18634−18641.
(22) Xi, C.; Marina, P. F.; Xia, H.; Wang, D. Directed Self-Assembly of Gold Nanoparticles into Plasmonic Chains. *Soft Matter* **2015**, *11*, 4562−4571.
(23) Ureta-Zañartu, M. S.; Berríos, C.; González, T.; Fernández, F.; Báez, D.; Salazar, R.; Gutiérrez, C. Electrocatalytic Oxidation of Alcohols at Gold Electrodes in Alkaline Media. *Int. J. Electrochem. Sci.* **2012**, *7*, 8905−8928.
(24) Wang, C.; Nie, X.-G.; Shi, Y.; Zhou, Y.; Xu, J.-J.; Xia, X.-H.; Chen, H.-Y. Direct Plasmon-Accelerated Electrochemical Reaction on Gold Nanoparticles. *ACS Nano* **2017**, *11*, 5897−5905.
(25) Sui, N.; Gao, H.; Zhu, J.; Jiang, H.; Bai, Q.; Xiao, H.; Liu, M.; Wang, L.; Yu, W. W. Shape- and Size-Dependences of Gold Nanostructures on the Electrooxidation of Methanol under Visible Light Irradiation. *Nanoscale* **2019**, *11*, 18320−18328.
(26) Huang, L.; Zou, J.; Ye, J. Y.; Zhou, Z. Y.; Lin, Z.; Kang, X.; Jain, P. K.; Chen, S. Synergy between Plasmonic and Electrocatalytic Activation of Methanol Oxidation on Palladium−Silver Alloy Nanotubes. *Angew. Chem., Int. Ed.* **2019**, *58*, 8794−8798.
(27) Jain, P. K. Taking the Heat off of Plasmonic Chemistry. *J. Phys. Chem. C* **2019**, *123*, 24347−24351.
(28) Shahbazyan, T. V. Landau Damping of Surface Plasmons in Metal Nanostructures. *Phys. Rev. B* **2016**, *94*, 235431.
(29) Ou, W.; Zhou, B.; Shen, J.; Lo, T. W.; Lei, D.; Li, S.; Zhong, J.; Li, Y. Y.; Lu, J. Thermal and Nonthermal Effects in Plasmon-Mediated Electrochemistry at Nanostructured Ag Electrodes. *Angew. Chem., Int. Ed.* **2020**, *59*, 6790−6793.
(30) Yu, Y.; Williams, J. D.; Willets, K. A. Quantifying Photothermal Heating at Plasmonic Nanoparticles by Scanning Electrochemical Microscopy. *Faraday Discuss.* **2018**, *210*, 29−39.
(31) Zhan, C.; Liu, B.-W.; Huang, Y.-F.; Hu, S.; Ren, B.; Moskovits, M.; Tian, Z.-Q. Disentangling Charge Carrier from Photothermal Effects in Plasmonic Metal Nanostructures. *Nat. Commun.* **2019**, *10*, 1−8.
(32) Bard, A. J.; Faulkner, L. R. *Electrochemical Methods: Fundamentals and Applications*, 2nd ed.; John Wiley & Sons, Inc., 2001.
(33) Rieth, A. J.; Gonzalez, M. I.; Kudisch, B.; Nava, M.; Nocera, D. G. How Radical Are "Radical" Photocatalysts? A Closed-Shell Meisenheimer Complex Is Identified as a Super-Reducing Photoreagent. *J. Am. Chem. Soc.* **2021**, *143*, 14352−14359.
(34) Yue, K.; Nan, J.; Zhang, X.; Tang, J.; Zhang, X. Photothermal Effects of Gold Nanoparticles Induced by Light Emitting Diodes. *Appl. Therm. Eng.* **2016**, *99*, 1093−1100.
(35) Wang, S.; Wang, C.; Ji, X. Towards Understanding the Salt-Intercalation Exfoliation of Graphite into Graphene. *RSC Adv.* **2017**, *7*, 52252−52260.
(36) Dovbeshko, G. I.; Romanyuk, V. R.; Pidgirnyi, D. V.; Cherepanov, V. V.; Andreev, E. O.; Levin, V. M.; Kuzhir, P. P.; Kaplas, T.; Svirko, Y. P. Optical Properties of Pyrolytic Carbon Films Versus Graphite and Graphene. *Nanoscale Res. Lett.* **2015**, *10*, 234.
(37) Biyikli, N.; Kimukin, I.; Butun, B.; Aytur, O.; Ozbay, E. ITO-Schottky Photodiodes for High-Performance Detection in the UV-IR Spectrum. *IEEE J. Sel. Top. Quantum Electron.* **2004**, *10*, 759−765.
(38) Dubi, Y.; Un, I. W.; Sivan, Y. Thermal Effects—An Alternative Mechanism for Plasmon-Assisted Photocatalysis. *Chem. Sci.* **2020**, *11*, 5017−5027.
(39) Yu, Y.; Sundaresan, V.; Willets, K. A. Hot Carriers versus Thermal Effects: Resolving the Enhancement Mechanisms for Plasmon-Mediated Photoelectrochemical Reactions. *J. Phys. Chem. C* **2018**, *122*, 5040−5048.
(40) Kishioka, S.-y.; Yamada, A. Electrooxidation of Vanillyl Alcohol in Acidic Aqueous Solution Using Rotating Ring-Disk Electrode Voltammetry. *Anal. Sci.* **2005**, *21*, 429−432.
(41) Delahay, P. Theory of Irreversible Waves in Oscillographic Polarography. *J. Am. Chem. Soc.* **1953**, *75*, 1190.
(42) Gileadi, E. *Physical Electrochemistry—Fundamentals, Techniques and Applications*, 2nd ed.; Wiley-VCH Verlag GmbH & Co., 2013.
(43) Rodriguez, P.; Koper, M. T. M. Electrocatalysis on Gold. *Phys. Chem. Chem. Phys.* **2014**, *16*, 13583−13594.
(44) Limon-Petersen, J. G.; Han, J. T.; Rees, N. V.; Dickinson, E. J. F.; Streeter, I.; Compton, R. G. Quantitative Voltammetry in Weakly Supported Media. Chronoamperometric Studies on Diverse One Electron Redox Couples Containing Various Charged Species: Dissecting Diffusional and Migrational Contributions and Assessing the Breakdown of Electroneutrality. *J. Phys. Chem. C* **2010**, *114*, 2227−2236.

NOTE ADDED AFTER ASAP PUBLICATION

This paper was originally published ASAP on March 18, 2022. Due to a production error, there was a mistake in eq 1. The corrected version was reposted on March 21, 2022.

https://doi.org/10.1021/acscatal.2c00206
ACS Catal. 2022, 12, 4110−4118